This article has been accepted for publication in a future issue of this journal, but has not been fully edited. Content may change prior to final publication. Citation information: DOI 10.1109/TNS.2021.3061209, IEEE Transactions on Nuclear Science

Assessment of proton direct ionization for the radiation hardness assurance of deep sub-micron SRAMs used in space applications

Andrea Coronetti, Rubén Garcìa Alìa, Jialei Wang, Maris Tali, Matteo Cecchetto, Carlo Cazzaniga, Arto Javanainen, Frédéric Saigné, and Paul Leroux

***Abstract*—Proton direct ionization from low-energy protons has been shown to have a potentially significant impact on the accuracy of prediction methods used to calculate the upset rates of memory devices in space applications for state-of-the-art deep sub-micron technologies. The general approach nowadays is to consider a safety margin to apply over the upset rate computed from high-energy proton and heavy ion experimental data. The data reported here present a challenge to this approach. Different upset rate prediction methods are used and compared in order to establish the impact of proton direct ionization on the total upset rate. No matter the method employed the findings suggest that proton direct ionization can contribute to up to 90% of the total upset rate on average for a general selection of space orbits, with peaks of up to 99%. Such results suggest that an approach based on the characterization of the low-energy portion of the proton spectrum would be more convenient for similar technologies than the application of a general safety margin. Based on data presented here, the previously proposed margin of 5 is exceeded, by large amounts in some cases.**

***Index Terms*—Radiation hardness assurance, low-energy protons, proton direct ionization, upset rate, space environment, prediction methodologies, Monte-Carlo simulations.**

I. Introduction

THE potential impact of direct ionization phenomena arising from singly charged particles, such as protons [1, 2], electrons [3] and muons [4], on the upset rate (UR) of memory devices has been a matter of concern for more than a decade. When it comes to space applications, low-energy protons (LEP) are one of the main threats challenging the standard UR prediction methodologies based on high-energy proton (HEP) and heavy ion (HI) single-event upset (SEU) characterizations. Although not specifying how to calculate the UR from low-energy protons, space standards for single event effects [5] are starting to mention procedures for SEU characterization under low-energy proton irradiation.

While it is common to refer to high-energy protons as those protons with energy above 20 MeV, the energy range for low-energy protons is not clearly defined. One of the reference studies in this subject [6] suggests to account only for protons having energies in the 0-3 MeV range because these are the only energies relevant for direct ionization. Such observation arose from those previous experimental observations.

An additional source of uncertainty on the total UR may arise from proton elastic scattering, occurring at energies below 20 MeV [7–9], which is generally neglected as well.

Both direct ionization and elastic scattering are phenomena that can cause SEUs in deep sub-micron technologies, no matter if they are based on bulk Si or silicon-on-insulator (SOI) processes [10]. Angular dependency was also shown to be an important factor for the triggering of SEU mechanisms. Normal incidence is considered worst-case for bulk silicon and 90° tilting worst-case for SOI [10].

SEUs from proton direct ionization (PDI) are triggered by the energy directly deposited by protons within the device sensitive volume (SV). This mechanism becomes more and more remarkable for those protons having an energy near the Bragg peak. That is, those protons that either stop within the SV or that pass through it while depositing most of their energy. These are protons that enter the SV with energies on the order of 50 keV.

In terms of radiation hardness assurance (RHA) for space missions, several approaches have been proposed in the past years for PDI UR predictions starting from ground test data [6, 10–13]. One of the main studies [6] proposes the use of a degraded high-energy proton beam as an enabler for low-energy proton SEU ground-testing. In this case, the main advantage is the possibility to exploit the energetic spread introduced by the degraders in the beamline to irradiate the device with a spectra replicating that found in a typical Earth space mission in the 0-3 MeV energy range.

The main conclusion of the study was that for static random access memories (SRAM) operated down to 10% under-voltage, the PDI contribution to the total UR could be counted by applying a conservative margin of 5 to the UR calculated from the conventional high-energy proton and heavy ion SEU

Manuscript received October 1, 2020.

This study has received funding from the European Union's Horizon 2020 research and innovation programme under the MSC grant agreement no. 721624 and in part by the European Space Agency (ESA/ESTEC) at the University of Jyväskylä under Contract 4000124504/18/NL/KML/zk

Andrea Coronetti (andrea.coronetti@cern.ch) is with CERN, CH-1211 Geneva 23, Switzerland and with the Department of Physics, University of Jyväskylä, 40014 Jyväskylä, Finland.

Rubén García Alía, Maris Tali and Matteo Cecchetto are with CERN, CH-1211 Geneva 23, Switzerland.

Jialei Wang and Paul Leroux are with KU Leuven, Department of Electrical Engineering (ESAT), 2440 Geel, Belgium.

Carlo Cazzaniga is with the Science and Technology Facility Council, OX11 0QX Didcot, UK.

Arto Javanainen is with Department of Physics, University of Jyväskylä, 40014 Jyväskylä, Finland and with the Electrical Engineering and Computer Science Department, Vanderbilt University, Nashville, TN 37235 USA.

Frédéric Saigné is with Institute d'Électronique et des Systèmes, Université de Montpellier, 34090 Montpellier, France.

This article has been accepted for publication in a future issue of this journal, but has not been fully edited. Content may change prior to final publication. Citation information: DOI 10.1109/TNS.2021.3061209, IEEE Transactions on Nuclear Science

TABLE I
SRAMS UNDER CONSIDERATION IN THIS WORK.

Name	Technology (nm)	Size (bits)	Core Voltage (V)
RADSAGA	65	32k	0.3
ISSI	40	32M	1.1
Cypress	65	16M	1.1

cross-sections determined through ground-testing [10].

The present work explores very strong PDI enhancements observed in the SEU cross-sections of a few SRAMs that can break the previous assumptions about the severity of PDI for space missions RHA. When considering the two commercial devices in the accelerator context [14], it was found that UR enhancements due to PDI up to a factor of 5 were expected. This despite the minor contribution of low-energy protons to the overall accelerator radiative environment (largely neutron dominated) if compared to the larger abundance of low-energy protons in the space environment. Thus, the objective is to determine whether the standard RHA approaches for PDI are challenged by this specific set of devices and by how much the previous safety margins might be violated.

This paper is structured as follows. The experimental investigation performed for this work is briefly introduced. The experimental data are fed into models to be used in Monte-Carlo (MC) simulation tools. These are used, along with other prediction tools to estimate the UR of the characterized devices for a few selected space orbits in order to evaluate the impact of PDI UR in typical space missions.

II. EXPERIMENTAL INVESTIGATION

One of the three characterized devices is a custom-developed SRAM designed by one of the authors of this paper and the other two are commercial SRAMs. The custom-developed SRAM will henceforth be referred as RADSAGA 65 nm SRAM. As the name suggests, it is based on a 65 nm technology and it was manufactured according to the standard commercial TSMC process. The only difference is that the cell size is three times larger than the standard. One of the commercially available SRAMs, reference CY62167GE30-45ZXI (henceforth called Cypress SRAM), is also based on this technology. The other commercial SRAM, reference IS61WV204816BLL-10TLI (henceforth called ISSI SRAM), is based on a 40 nm technology. The main features of these memories are summarized in Table I.

Note that the RADSAGA 65 nm SRAM [15] has a tunable core voltage that can be used to vary the sensitivity of the memory chip, spanning in the 0.3-1.2 V range. For the scope of this paper, the presented data and the main focus will be devoted to a core voltage of 0.3 V. The data presented for the commercial SRAMs all refer to their nominal core-voltages of 1.1 V. Note that the Cypress SRAM has an internal error-correction code (ECC), which has been disabled for the purposes of this study.

The SRAMs have been tested with several beams [16] and most of the experimental details are reported in that paper. All the SRAMs have been irradiated through the back-end-of-line (BEOL). This was shown to have an impact for SOI SRAMs [17] with respect to an irradiation from the substrate. For the presented bulk SRAMs, however, such configuration could not be achieved.

TABLE II
MAIN CHARACTERISTICS OF THE HEAVY IONS USED TO CHARACTERIZE THE SEU CROSS-SECTIONS.

Ion	Energy (MeV)	LET (MeV/(mg/cm^2))	Range (mm)
C	1080	0.22	11.78
C	720	0.31	5.73
C	360	0.52	1.67
Ar	1050	5.2	0.55
Ar	548	8.1	0.20
Xe	2700	43.5	0.22

For the purpose of this work, data referring to low- and high-energy proton and heavy ion irradiations are reported. Concerning low-energy protons, the core of the experimental work was completed at the Centro Nacional de Aceleradores (CNA) [18]. There, the SRAMs have been irradiated with mono-energetic proton beams in the 0.5-5 MeV energy range. Low-energy proton data for the ISSI SRAM were collected at the Radiation Effects Facility (RADEF) [19, 20] at the University of Jyväskylä. High-energy proton testing was accomplished at the Kernfysisch Versneller Instituut (KVI) [21] for the ISSI and Cypress SRAMs and at the Paul Scherrer Institute (PSI) [22] for the RADSAGA 65 nm SRAM. Heavy ion testing was performed at KVI for all the SRAMs. Table II reports the heavy ion characteristics in terms of species, energy, LET and range. Only the low-energy proton testing at CNA and RADEF were performed in vacuum. All the data have been obtained at normal incidence and room temperature. Differently from other experiments and measurement techniques [23, 24], mono-energetic low-energy proton data have not been obtained by beam degradation.

Error bars for all experimental data are calculated at 95% confidence level assuming a fluence uncertainty of 10% and based on the actual number of events. If not visible in the plots, they are smaller than the markers.

The experimental proton cross-sections as a function of energy for the RADSAGA 65 nm SRAM are depicted in Fig. 1. The peak direct ionization cross-section was found for 900 keV and it reaches up to 4 x 10^{-9} cm^2/bit. The cross-section is still higher than 10^{-12} cm^2/bit at 5 MeV. The high-energy proton cross-section lowers down to 1.5 x 10^{-13} cm^2/bit at 200 MeV. It is seen to grow from below 100 MeV to reach up to 4.7 x 10^{-13} cm^2/bit at 18 MeV. This may indicate a potential influence of direct ionization at energies around 20 MeV. For the Weibull fit the saturation cross-section is taken to be 1.8 x 10^{-13} cm^2/bit to better account for this enhancement below 100 MeV. Overall, the peak PDI cross-section is about 2.2 x 10^4 times the high-energy proton saturation cross-section used for the Weibull fit.

The experimental proton cross-sections as a function of energy for the ISSI SRAM are depicted in Fig. 2. The peak direct ionization cross-section was observed at 600-800 keV, probably indicating a thinner BEOL than the previous SRAM.

This article has been accepted for publication in a future issue of this journal, but has not been fully edited. Content may change prior to final publication. Citation information: DOI 10.1109/TNS.2021.3061209, IEEE Transactions on Nuclear Science

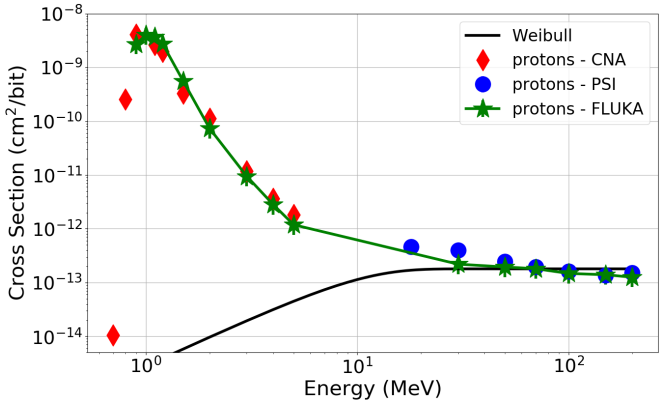

Fig. 1. Low- and high-energy proton experimental cross-sections as a function of proton energy for the RADSAGA 65 nm SRAM when tuned at 0.3 V. The high-energy proton data are fitted with a Weibull with the following parameters: σ_{sat} = 1.8 x 10^{-13} cm^2/bit, E_0 = 0 MeV, W = 10 MeV, s = 1.8. The data are compared with the FLUKA simulated cross-sections.

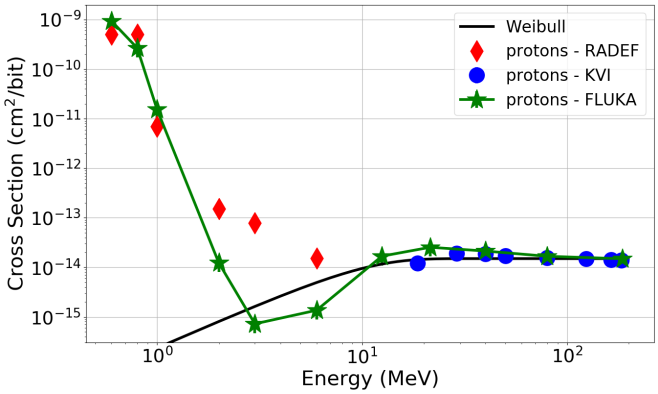

Fig. 2. Low- and high-energy proton experimental cross-sections as a function of proton energy for the ISSI SRAM. The high-energy proton data are fitted with a Weibull with the following parameters: σ_{sat} = 1.5 x 10^{-14} cm^2/bit, E_0 = 10 MeV, W = 0 MeV, s = 1.8. The data are compared with the FLUKA simulated cross-sections.

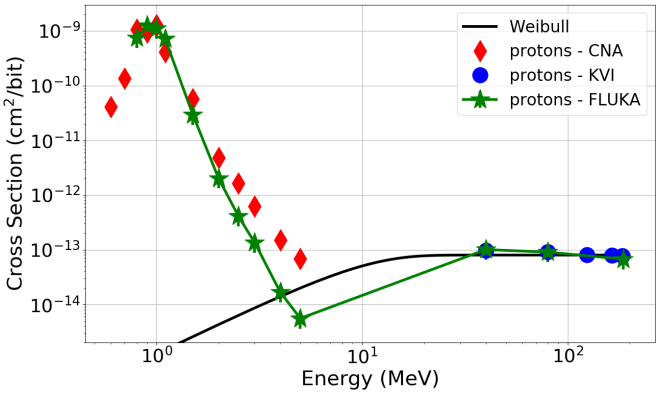

Fig. 3. Low- and high-energy proton experimental cross-sections as a function of proton energy for the Cypress SRAM. The high-energy proton data are fitted with a Weibull with the following parameters: σ_{sat} = 8 x 10^{-14} cm^2/bit, E_0 = 10 MeV, W = 0 MeV, s = 1.8. The data are compared with the FLUKA simulated cross-sections.

The fact that the LEP cross-section is almost constant for an interval of energies (600-800 keV) more strongly points out the reaching of the physical limit imposed by the SV size. The peak cross-section is 5 x 10^{-10} cm^2/bit. The high-energy proton saturation cross-section is 1.5 x 10^{-14} cm^2/bit, resulting in a ratio between the peak PDI and high-energy saturation cross-sections of 3.3 x 10^4.

The indicated ratios are among the highest that could be found in the literature. In one case [25], ratios up to a factor of 10^5-10^6 were observed. However, differently from these data, the peaks were quite steep and narrow, indicating a higher critical charge than for the devices here considered.

The experimental proton cross-sections as a function of energy for the Cypress SRAM are depicted in Fig. 3. The peak direct ionization cross-section is seen to occur between 800 keV and 1 MeV, stretching up to 1.2 x 10^{-9} cm^2/bit. The high-energy proton saturation cross-section is 8 x 10^{-14} cm^2/bit. As a result, the ratio between the peak PDI and high-energy saturation cross-sections is 1.5 x 10^4.

Fig. 4 presents the same PDI data for the RADSAGA 65 nm SRAM as a function of linear energy transfer (LET) compared to cross-sections obtained with long range ions. Other than the data points at high-LET, which define the heavy ion saturation cross-section, the main purpose of the figure is to compare the cross-sections of low-energy protons with those of long range high-energy light ions (carbon in the 30-90 MeV/u energy range).

In the figure, ion data-points have been placed at an LET corresponding to that before the BEOL. It is assumed that, given their longer range, the ions will reach the SV while losing a negligible amount of energy in the BEOL. On the contrary, low-energy protons have a shorter range that may bring them to stop either inside the SV or in its vicinity. Thus, low-energy proton data-points have not been placed at the tabulated LET [26] for that primary energy before the BEOL. A more realistic LET has been estimated based on the interaction with the BEOL. While the latter cannot be known for the commercial memories, the experimental cross-section helped deducing their SiO_2 equivalent BEOL thicknesses. On the other hand, for the RADSAGA 65 nm SRAM it is known from manufacturing documentation that the BEOL would be equivalent to a layer of SiO_2 12 μm thick.

Whether known or deduced from the data, this equivalent thickness was used to calculate the energy lost by the primary protons while passing through the BEOL by means of the SRIM software [27]. Once this was known, SRIM was again used to determine the range in silicon of a proton having the residual kinetic energy and calculate a LET based on this residual kinetic energy and the range. This LET is exclusively used to show the low-energy proton points in the plots.

Note that this method introduces an approximation, since it considers that all the protons transiting through the BEOL will experience the same identical energy loss. FLUKA 4.0 [28, 29] was used to simulate mono-energetic 900 keV protons travelling through the BEOL oxide. Due to straggling, the resulting spectra after the BEOL and at the entry of the SV were found to be continuous between 0 and 200 keV. This was also observed in [30]. At the same time, the residual kinetic energy obtained from SRIM for this case was about

This article has been accepted for publication in a future issue of this journal, but has not been fully edited. Content may change prior to final publication. Citation information: DOI 10.1109/TNS.2021.3061209, IEEE Transactions on Nuclear Science

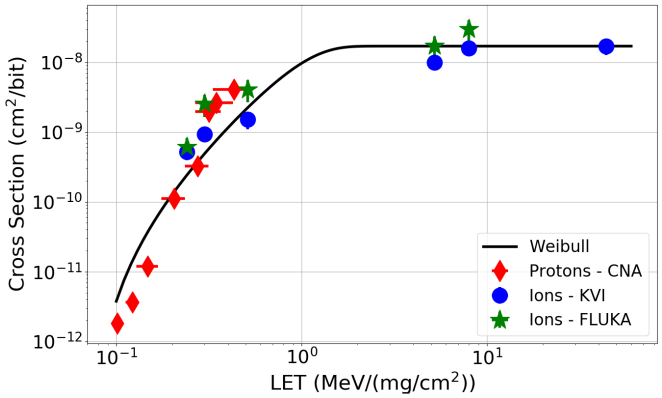

Fig. 4. Low-energy proton and heavy ion cross-sections as a function of LET for the RADSAGA 65 nm SRAM when tuned at 0.3 V. Weibull parameters: σ_{sat} = 1.7 x 10^{-8} cm^2/bit, LET$_0$ = 0.07 MeV/(mg/cm^2), W = 1 MeV/(mg/cm^2), s = 2.4. The data are compared with the FLUKA simulated cross-sections.

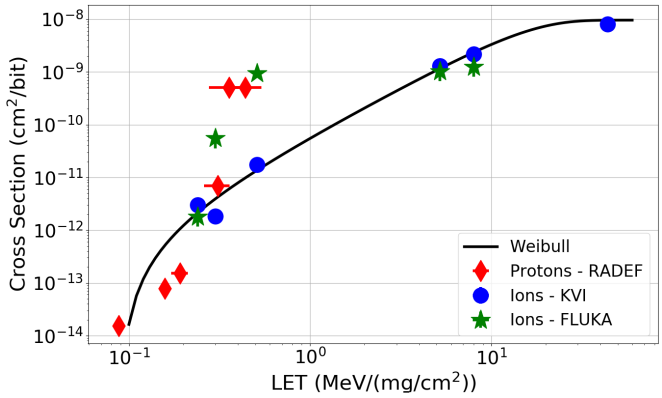

Fig. 5. Low-energy proton and heavy ion cross-sections as a function of LET for the ISSI SRAM. Weibull parameters: σ_{sat} = 9.56 x 10^{-9} cm^2/bit, LET$_0$ = 0.09 MeV/(mg/cm^2), W = 16 MeV/(mg/cm^2), s = 1.8. The data are compared with the FLUKA simulated cross-sections.

290 keV. Considering the energy straggling, using a single LET derived from a single proton energy may result in an underestimation of the LET of less than 0.1 MeV/(mg/cm^2), which will not alter the general picture.

Coming back to Fig. 4, it is clear that the peak PDI cross-sections are not fully reproduced by long range light ions, as was found before [31]. In this case, the peak PDI cross-section can be three times higher than the respective carbon cross-section at a similar LET.

Fig. 5 shows the low-energy proton and heavy ion cross-sections as a function of LET for the ISSI SRAM. The same procedure, as for the previous case, was implemented for the low-energy proton LET determination, this time with a BEOL as thick as 6 μm. The PDI peak is seen to exceed the carbon cross-sections for similar LET by even a factor of 50. Indeed, the peak PDI cross-sections are even closer to the argon ion cross-sections obtained with LETs above 5 MeV/(mg/cm^2) than to the carbon ion cross-sections.

Fig. 6 depicts the low-energy proton and heavy ion cross-sections as a function of LET for the Cypress SRAM. The LETs for low-energy protons were calculated assuming a

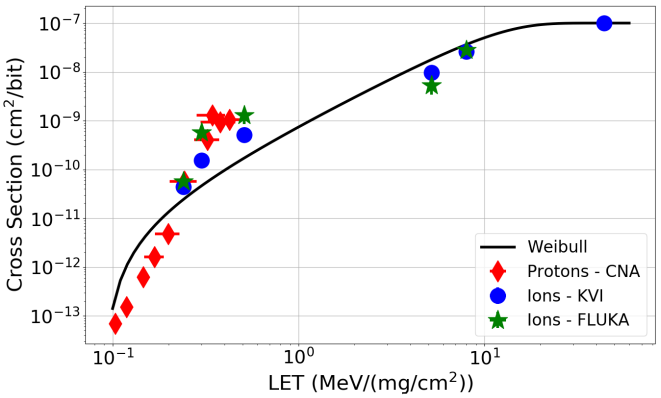

Fig. 6. Low-energy proton and heavy ion cross-sections as a function of LET for the Cypress SRAM. Weibull parameters: σ_{sat} = 1 x 10^{-7} cm^2/bit, LET$_0$ = 0.09 MeV/(mg/cm^2), W = 12 MeV/(mg/cm^2), s = 1.9. The data are compared with the FLUKA simulated cross-sections.

BEOL 10 μm thick. This was chosen because the PDI peak cross-section is maximum between 0.8-1 MeV and it starts fading only below 800 keV. Hence, at an energy lower than where the fading is observed for the RADSAGA 65 nm SRAM. The situation is similar to the RADSAGA 65 nm SRAM, with a maximum difference among peak PDI and carbon ion cross-sections of a factor of 3.

The reason for the observed experimental behaviors is not fully clear, but it is not caused by the presence of Multiple-Bit Upsets (MBU, occurring in the same word), while nothing can be said about Multiple-Cell Upsets (MCU, occurring in physically adjacent cells) given that the physical mapping of the memories is not available. It may be a topic of future investigations. The presented heavy ion LET Weibull functions are derived to follow the heavy ion data at both low- and high-LET and will be later used to calculate the heavy ion contributions to the total UR.

Carbon and argon ion interactions were also simulated with FLUKA and are reported in the figures. For all the models the FLUKA simulated cross-sections for carbon (low-LET) tend to follow the low-energy proton experimental data rather than the carbon experimental data at similar LET. This is particularly evident for the ISSI SRAM (Fig. 5). On the other end, the agreement between argon experimental data and simulated data is within a factor of 2 for all the models.

III. Modeling of the Sensitive Volumes

SV models are proposed for the memory cells of the three SRAMs. They will be used as input in the Monte-Carlo simulations used to determine the UR of the SRAMs in the space environment.

All the SRAM models here considered are based on Rectangular ParallelePiped (RPP) that are built based on the experimental data. Low-energy proton data are very useful when building such models since they can give direct indications of the SV size, i.e., the direct ionization cross-section tends to be equal to the SV surface normal to the beam. In addition, the lowering of the cross-section at energies below the PDI peak can give indications about the BEOL thickness. Finally, the

This article has been accepted for publication in a future issue of this journal, but has not been fully edited. Content may change prior to final publication. Citation information: DOI 10.1109/TNS.2021.3061209, IEEE Transactions on Nuclear Science

TABLE III
NESTED RPP DATA OF THE SVS OF EACH SRAM ALONG WITH THE COLLECTION EFFICIENCY (ALPHA), BEOL THICKNESS AND CRITICAL CHARGE.

RADSAGA 65 nm SRAM		
BEOL 12 μm, Q_{crit} = 0.55 fC		
SV side (nm)	**SV thickness (nm)**	**alpha**
638	250	1
996	250	0.077
1304	250	0.050
ISSI SRAM		
BEOL 6 μm, Q_{crit} = 0.96 fC		
SV side (nm)	**SV thickness (nm)**	**alpha**
310	310	1
Cypress SRAM		
BEOL 10 μm, Q_{crit} = 0.86 fC		
SV side (nm)	**SV thickness (nm)**	**alpha**
360	360	1
984	360	0.057
1612	360	0.037
3160	360	0.007

TABLE IV
COMPARISON OF THE ENERGY CONVOLUTION OF THE EXPERIMENTAL AND RPP MODEL PROTON RESPONSES FOR LOW- (0-3 MEV), INTERMEDIATE (3-20 MEV) AND HIGH-ENERGY (> 20 MEV) REGIONS FOR THE THREE SRAMS WITH THE ISS ENVIRONMENT AND 100 MILS OF ALUMINUM SHIELDING. DATA ARE REPORTED IN SEU/BIT/DAY.

Data	**0-3 MeV**	**3-20 MeV**	**> 20 MeV**	**Total**
RADSAGA 65 nm SRAM				
Exp	8.00 x 10^{-6}	4.37 x 10^{-7}	5.90 x 10^{-7}	9.03 x 10^{-6}
RPP	9.06 x 10^{-6}	2.94 x 10^{-7}	4.59 x 10^{-7}	9.81 x 10^{-6}
ISSI SRAM				
Exp	6.22 x 10^{-7}	5.38 x 10^{-9}	4.14 x 10^{-8}	6.69 x 10^{-7}
RPP	6.76 x 10^{-7}	3.80 x 10^{-9}	4.53 x 10^{-8}	7.25 x 10^{-7}
Cypress SRAM				
Exp	1.89 x 10^{-6}	2.34 x 10^{-8}	2.22 x 10^{-7}	2.14 x 10^{-6}
RPP	2.11 x 10^{-6}	7.64 x 10^{-9}	2.08 x 10^{-7}	2.33 x 10^{-6}

slope of the cross-section curve from the PDI peak towards higher energies can give indications about the SV thickness and the critical charge Q_{crit} [14].

Even when these low-energy proton data are correctly fitted, often a single RPP can be representative of the low-energy proton cross-section, but it can underestimate the high-energy proton cross-section. Given that the models will be used for the estimations of the UR due to low- and high-energy protons, as well as heavy ions, it is crucial to build models that could reproduce in the best possible way also the high-energy part of the proton cross-section. A nested RPP technique [11, 32] based on heavy ion data can be used to better fit the high-energy proton cross-section while not affecting the low-energy part.

The nested RPP technique was used for the RADSAGA 65 nm and Cypress SRAMs. On the other hand, a single RPP was found to be suitable for the ISSI SRAM since it fairly reproduces both the low- and high-energy proton responses. The data of the RPP models for all the SRAMs are reported in Table III. The BEOL are assumed to be made with SiO_2 for all the cases.

For the nested RPPs, the external volume sides are obtained directly by a few high-LET heavy ion ($>$ 5 MeV/(mg/cm^2)) cross-section data-points. The collection efficiency (alpha) is obtained by making the ratio between the LET of the PDI peak data-point and the LET of that heavy ion. For the RADSAGA 65 nm SRAM the reference proton LET is 0.4 MeV/(mg/cm^2), whereas for the Cypress SRAM this is 0.3 MeV/(mg/cm^2). The thickness is kept constant [33] and equal to that of the innermost SV (targeted to reproduce the PDI enhancement).

The RADSAGA 65 nm SRAM has the largest SV side (640 nm) for the innermost volume. At the same time, this is the only model for which the SV thickness (250 nm) did not coincide with the SV side. The reason is the matching of the proton cross-section at energies of 1-5 MeV. Using a larger thickness would lead the simulated cross-section to fall down much quicker with increasing energy. The critical charge is also the lowest (0.55 fC), given the lower core voltage. For the outermost volumes, only the argon ion data are retained, since the Xe data-point has the same cross-section as the argon ion with the highest LET.

The ISSI SRAM has the lowest PDI peak cross-section, hence the lowest RPP side (310 nm). It also has the thinner BEOL (6 μm) since the memory was experimentally observed to be sensitive down to just 600 keV. Finally, it also relies on the highest critical charge (0.96 fC), which, in spite of the smaller technology, is likely due to differences in the manufacturing processes among companies.

For the innermost volume, the Cypress SRAM model has SV side and thickness of 360 nm. The critical charge is 0.86 fC. To complete the model, three larger volumes are added based on the argon and xenon cross-sections. In this case, the heavy ion saturation cross-section is much larger than that of the RADSAGA 65 nm SRAM, resulting in volumes with sides as large as 3 μm.

FLUKA Monte-Carlo simulations were performed for all the models and for several mono-energetic proton cases to assess the consistency of the model with respect to the experimental data. The uncertainty on the calculated cross-sections varies with each energy. On average, an uncertainty of $\pm$ 35% can be taken for all the data points and models based on the energy deposition distributions. Other uncertainties may be present on the parameters chosen for the SV such as BEOL thickness, critical charge, SV size and thickness.

Figs. 1-3 present the comparison among the mono-energetic experimental and simulated cross-sections for the RADSAGA 65 nm SRAM, ISSI SRAM and Cypress SRAM, respectively.

For the RADSAGA 65 nm SRAM the consistency is verified at low- (0-3 MeV), intermediate- (3-20 MeV) and high-energy ($>$ 20 MeV). For the ISSI and Cypress SRAM the agreement between the models and the experiments is good for low- and high-energy protons. For the intermediate-energy region the agreements are less optimal. However, this region is not an important contributor when it comes to the proton UR since it contributes less than 1%, at least for these two SRAMs.

As a further verification of the validity of the proposed RPP models to describe the proton cross-section response over different sets of energies, a first UR calculation was performed. CREME96 [34] was used to determine the trapped proton flux

This article has been accepted for publication in a future issue of this journal, but has not been fully edited. Content may change prior to final publication. Citation information: DOI 10.1109/TNS.2021.3061209, IEEE Transactions on Nuclear Science

for the International Space Station (ISS) orbit. The flux was transported by means of the online tool through 100 mils of Aluminum. The data were then divided into the three energy regions described before. Both the experimental data and the RPP model data were convolved along with the proton fluxes in the three energy regions. Both data-sets are determined for normal incidence only, for both the data and the radiation field. For this simple calculation, the angular response is not considered because no such experimental data were collected and a fair comparison would not be possible.

Table IV reports the comparison for all three devices and for each energy region. The agreement for each region is quite satisfactory. The largest discrepancies are seen for the ISSI and Cypress SRAMs for intermediate-energy protons. However, given that, for these memories, this region is expected to contribute 1% or less to the total UR, the related inaccuracy can be assumed to be negligible. Globally, the total URs from these models are about 10% higher than their experimental counterparts.

TABLE V
COMPARISON OF UR PREDICTION METHODS FOR LOW- AND HIGH-ENERGY PROTONS AND HEAVY IONS FOR THE THREE SRAMS AT 0.3 V FOR THE LISTED METHODS. THE ISS ENVIRONMENT IS USED FOR ALL METHODS (500 KM, 51.6°, SOLAR MIN, 100 MILS ALUMINIUM). THE UR UNITS ARE SEU/BIT/DAY.

RADSAGA 65 nm SRAM			
Method	**High-E protons**	**Low-E protons**	**Heavy ions**
Energy convolution	5.42 x 10^{-7}	8.49 x 10^{-6}	X
Weibull	4.57 x 10^{-7}	X	2.65 x 10^{-7}
Monte-Carlo	3.04 x 10^{-7}	1.47 x 10^{-5}	4.07 x 10^{-7}
Approx. Dodds'	4.57 x 10^{-7}	1.43 x 10^{-5}	2.65 x 10^{-7}
ISSI SRAM			
Method	**High-E protons**	**Low-E protons**	**Heavy ions**
Energy convolution	4.06 x 10^{-8}	6.27 x 10^{-7}	X
Weibull	3.81 x 10^{-8}	X	3.90 x 10^{-9}
Monte-Carlo	2.33 x 10^{-8}	5.76 x 10^{-7}	5.34 x 10^{-8}
Approx. Dodds'	3.81 x 10^{-8}	1.20 x 10^{-6}	3.90 x 10^{-9}
Cypress SRAM			
Method	**High-E protons**	**Low-E protons**	**Heavy ions**
Energy convolution	2.25 x 10^{-7}	1.92 x 10^{-6}	X
Weibull	2.03 x 10^{-7}	X	4.02 x 10^{-8}
Monte-Carlo	1.58 x 10^{-7}	1.88 x 10^{-6}	1.10 x 10^{-7}
Approx. Dodds'	2.03 x 10^{-7}	3.41 x 10^{-6}	4.02 x 10^{-8}

IV. UPSET RATE PREDICTION METHODS

Upset rate prediction methods based on the measurements of high-energy proton and heavy ion cross-sections are nowadays well standardized, e.g., the Weibull [35] method, among others. Existing methods on high-energy protons and heavy ions are all based on the assumptions made from the typical test results that cross-section curves are null below the energy/LET threshold and tend to reach a saturation cross-section at high-energy/LET while maintaining a monotonic dependency with energy/LET.

PDI, however, introduces the problem that the cross-section is no longer monotonic with energy. Hence, the established prediction methods can hardly help out in predicting the UR from low-energy protons. In principle, some of these methods can be mimicked in some other way, because they are basically convolutions of a cross-section function defined as a function of energy/LET with an environmental particle spectrum, similarly defined as a function of energy/LET.

The low-energy proton experimental mono-energetic cross-sections can, for instance, be convolved with the environmental flux without a need to define a function that would describe the whole cross-section curve as a function of energy, i.e., by performing linear interpolation for intermediate points. This is supposed to provide a more accurate estimation than that obtained by multiplying the cross-section peak for the proton flux in the relevant energy range, as proposed in [36].

Still, among the problems introduced by energy convolution, there is the assumption that the proton will reach the sensitive volume with normal incidence, which is not the case since the space environmental proton fluxes are isotropic. For instance, when folding the cross-sections presented in Fig. 1, all protons within the environment having an energy below 700 keV will not contribute to the response. However, when considering an isotropic spectrum, there will always be protons arriving at the SV with an energy in the 0-700 keV range, which, in principle, are associated with a cross-section similar with that of the PDI peak. Such a method, based on the energy and range of protons arriving at the SV, was also proposed in the past [37].

Another possibility would be to treat the low-energy protons in a similar fashion as heavy ions and to perform a LET convolution. However, in this case, determining the LET of the protons used during the experiments can, as was shown before, be complicated and the uncertainty introduced by the straggling may lead to much higher inaccuracy than for the determination of the actual proton energy.

A promising method, proposed by Dodds [6], to calculate the UR from PDI consists of measuring the cross-section of a degraded high-energy beam containing a known spectrum of low-energy protons. The method also requires performing measurements at various angles of incidence to cover the effects related to the isotropic nature of the space spectra. The PDI UR is then compared to those attained through the Weibull method for high-energy protons and heavy ions. However, when data from such an experiment are not available, approximate methods may be introduced based on the observed mono-energetic proton cross-sections in order to retrieve the UR.

Finally, Monte-Carlo simulations can also be considered for UR predictions. The earlier introduced RPP models of the SV can be used to extract the cross-sections derived from the environmental proton and heavy ion spectra. The advantage of MC simulations is that the models used are assumed to be a valid representation of the device response no matter the particle or energy. In addition, they may also provide further indications about potential variations introduced by varying the parameters in the chosen models. Note that the MC simulations are run with isotropic spectra as input, hence accounting for the angular response of the modelled component. A certain degree of uncertainty, which is not so easy to quantify, is present, anyhow. This is due to the lack of experimental data at different angles of incidence. That is,

the angular dependency here considered is that emerging as a result of the modelling at normal incidence, but no verification with respect to experimental data was possible.

For this first assessment, the data refer to a single orbit and a single shielding configuration. The environment under consideration is that of the ISS for solar minimum conditions. Both proton and heavy ion fluxes are transported through 100 mils of Aluminum with the CREME/UPROP online tool. The fluxes are then used to perform energy convolution calculations (applicable only to protons), the Weibull fit calculations (applicable only to high-energy protons and heavy ions), FLUKA MC simulations (applicable to every particle and energy) and an approximated Dodds' method (applicable only to low-energy protons).

For the heavy-ion Weibull methods, the Weibull curves presented in Figs. 4-6 were used. For the high-energy protons, the same identical Weibull functions were used for the three devices, but with a different saturation cross-section (E_{th} = 0 MeV, W = 10 MeV, s = 1.8). The saturation cross-sections were 1.8 x 10^{-13}, 1.5 x 10^{-14} and 8 x 10^{-13} cm^2/bit for the RADSAGA 65 nm, ISSI and Cypress SRAMs, respectively (Figs. 1-3).

The idea behind the approximated Dodds' method is to retrieve a rough estimate of the cross-section that would have been measured for the devices presented in this work if experimental measurements in a high-energy degraded beam were performed. Note that the Dodds' method can be used to calculate the LEP contribution to the UR, whereas for the HEP and HI contributions the method also relies on the Weibull fits.

The approximated Dodds' method consists in the convolution of the experimental low-energy proton cross-section with the spectrum experimentally measured at TRIUMF [6] when degrading the 70 MeV proton beam to an average energy of 6 MeV. Once this cross-section is estimated, the approximated method follows the same steps as the original Dodds' method.

Table V presents the UR calculated for the three contributors: low- and high-energy protons and heavy ions with the various methods. Note that in this case all protons in the environment below 20 MeV are considered as low-energy protons, as they are typically irrelevant in the traditional methods based on high-energy proton and heavy ion characterizations only.

For all three devices the energy convolution, Weibull and MC methods deliver very similar high-energy proton URs, always within less than a factor of 2 difference. For heavy ions the Weibull and the MC methods are quite in disagreement for the ISSI SRAM, with even one order of magnitude lower UR delivered by the Weibull fit. For the other two SRAMs, the differences are much smaller, within a factor of 1.5 for the RADSAGA 65 nm SRAM and less than a factor of of 3 for the Cypress SRAM. The larger HI UR arising from MC simulations is due to the fact that the RPP models of the SVs are built so that they follow the experimental low-energy proton cross-sections at low-LET rather than the light ion cross-sections. As was earlier shown, the difference is not negligible, in particular for the ISSI SRAM, for which the discrepancy between different heavy ion UR estimation methods is the highest.

Concerning the comparison among low-energy proton UR prediction methods, the results are not always consistent among devices. For the RADSAGA 65 nm SRAM the energy convolution delivers a UR which is about half that of the MC simulations and the approximated Dodds' method, which, in turn, are very similar. This effect may be related to the isotropic nature of the environment, which is neglected in the energy convolution method. However, although this is indeed always the case for all the memories when comparing energy convolution and approximated Dodds' method, for the ISSI and Cypress SRAMs the MC low-energy proton UR is similar to that obtained through energy convolution.

Since the combined Weibull/Dodds' method and the MC simulations provide data for all three contributors to the total UR, these two approaches are followed to perform the following RHA assessments. One of the main differences between the two methods is that the approximated Dodds' method considers only protons with energy below 3 MeV, whereas the MC simulations consider the full proton spectra below 20 MeV.

V. Proton Direct Ionization Impact on the Total Upset Rate

Generally, the UR of a digital device in any space orbit is defined by two main contributions, i.e., direct heavy ion ionization and proton indirect ionization. PDI can be considered as a separate contributor since the proton-induced SEUs are, in this case, triggered similarly to those from heavy ions. In order to evaluate the impact of PDI on the total UR, let's define a parameter D as:

$$D = \frac{UR_{HI} + UR_{HEP} + UR_{LEP}}{UR_{HI} + UR_{HEP}} \quad (1)$$

The D-factor will define the relative contribution of PDI to the UR with respect to the UR estimated when PDI is neglected. It can also be seen as a safety margin to apply to the estimated UR when LEP data are not available.

The analysis is made considering the three devices presented in this paper, four different space radiation environments and two different shielding configurations. All the environments are calculated through the CREME96 online tools. The ISS environment (I1 and I5) is calculated at 500 km altitude, 51.6° inclination, solar minimum, quiet conditions; the LEO environment (L1 and L5) at 1400 km altitude, 52°, solar minimum, quiet conditions; the GEO environment is calculated for both quiet (GQ1 and GQ5) and stormy solar conditions (GW1 and GW5, worst day). The shielding configurations are with 100 and 500 mils of Aluminum.

For the RADSAGA 65 nm SRAM the contributions to the UR (both in absolute and percentage terms) are reported in Table VI for both the MC simulations and for the approximated Dodds' method. PDI effects are found to be negligible only for the GEO quiet conditions, for which both methods, no matter the shielding, yield a PDI UR in the order of 1%. For all other radiation environments, the PDI contribution to the UR is never below 85%. The most affected orbits are the LEO and GEO in stormy conditions and the situation does not change much when a thicker shielding is considered. Generally, the two methods yield very similar results for the PDI contribution

This article has been accepted for publication in a future issue of this journal, but has not been fully edited. Content may change prior to final publication. Citation information: DOI 10.1109/TNS.2021.3061209, IEEE Transactions on Nuclear Science

TABLE VI
UR OF THE **RADSAGA 65 NM SRAM** FROM PROTON INDIRECT AND DIRECT IONIZATION AND HEAVY IONS (WITH PERCENTAGE CONTRIBUTIONS TO THE TOTAL UR IN BRACKETS) FOR EIGHT COMBINATIONS OF ORBITS AND SHIELDING CONFIGURATIONS. UR IN SEU/BIT/DAY.

Monte-Carlo			
Env.	**UR$_{HEP}$ (%)**	**UR$_{LEP}$ (%)**	**UR$_{HI}$ (%)**
I1	3.04 x 10^{-7} (2%)	1.47 x 10^{-5} (96%)	2.65 x 10^{-7} (2%)
I5	2.41 x 10^{-7} (6%)	3.72 x 10^{-6} (89%)	2.39 x 10^{-7} (6%)
L1	2.38 x 10^{-5} (2%)	1.03 x 10^{-3} (98%)	3.98 x 10^{-7} (0%)
L5	7.72 x 10^{-6} (4%)	2.07 x 10^{-4} (96%)	3.59 x 10^{-7} (0%)
GQ1	3.94 x 10^{-8} (2%)	1.89 x 10^{-8} (1%)	1.84 x 10^{-6} (97%)
GQ5	4.09 x 10^{-8} (3%)	1.79 x 10^{-8} (1%)	1.46 x 10^{-6} (96%)
GW1	3.92 x 10^{-4} (0%)	1.44 x 10^{-1} (96%)	6.04 x 10^{-3} (4%)
GW5	5.98 x 10^{-5} (1%)	5.04 x 10^{-3} (98%)	6.27 x 10^{-5} (1%)
Approximated Dodds' method			
Env.	**UR$_{HEP}$ (%)**	**UR$_{LEP}$ (%)**	**UR$_{HI}$ (%)**
I1	4.57 x 10^{-7} (3%)	1.43 x 10^{-5} (95%)	2.65 x 10^{-7} (2%)
I5	3.32 x 10^{-7} (9%)	3.32 x 10^{-6} (85%)	2.39 x 10^{-7} (6%)
L1	2.29 x 10^{-5} (2%)	9.79 x 10^{-4} (98%)	3.98 x 10^{-7} (0%)
L5	1.64 x 10^{-5} (9%)	1.76 x 10^{-4} (91%)	3.59 x 10^{-7} (0%)
GQ1	5.96 x 10^{-8} (3%)	1.48 x 10^{-8} (1%)	1.84 x 10^{-6} (96%)
GQ5	5.77 x 10^{-8} (4%)	1.72 x 10^{-8} (1%)	1.46 x 10^{-6} (95%)
GW1	3.89 x 10^{-4} (0%)	1.36 x 10^{-1} (96%)	6.04 x 10^{-3} (4%)
GW5	9.65 x 10^{-5} (2%)	4.94 x 10^{-3} (97%)	6.27 x 10^{-5} (1%)

TABLE VII
UR OF THE **ISSI SRAM** FROM PROTON INDIRECT AND DIRECT IONIZATION AND HEAVY IONS (WITH PERCENTAGE CONTRIBUTIONS TO THE TOTAL UR IN BRACKETS) FOR EIGHT COMBINATIONS OF ORBITS AND SHIELDING CONFIGURATIONS. UR IN SEU/BIT/DAY.

Monte-Carlo			
Env.	**UR$_{HEP}$ (%)**	**UR$_{LEP}$ (%)**	**UR$_{HI}$ (%)**
I1	2.33 x 10^{-8} (4%)	5.76 x 10^{-7} (96%)	3.90 x 10^{-9} (1%))
I5	3.94 x 10^{-8} (32%)	8.13 x 10^{-8} (65%)	3.45 x 10^{-9} (3%)
L1	2.47 x 10^{-6} (6%)	4.00 x 10^{-5} (94%)	5.77 x 10^{-9} (0%)
L5	8.27 x 10^{-7} (14%)	5.54 x 10^{-6} (86%)	5.14 x 10^{-9} (0%)
GQ1	6.01 x 10^{-9} (14%)	2.50 x 10^{-9} (6%)	3.50 x 10^{-8} (80%)
GQ5	2.40 x 10^{-9} (8%)	3.44 x 10^{-9} (11%)	2.49 x 10^{-8} (81%)
GW1	8.81 x 10^{-5} (2%)	5.04 x 10^{-3} (97%)	4.46 x 10^{-5} (1%)
GW5	8.62 x 10^{-6} (4%)	4.14 x 10^{-4} (96%)	4.35 x 10^{-7} (0%)
Approximated Dodds' method			
Env.	**UR$_{HEP}$ (%)**	**UR$_{LEP}$ (%)**	**UR$_{HI}$ (%)**
I1	3.81 x 10^{-8} (3%)	1.20 x 10^{-6} (97%)	3.90 x 10^{-9} (0%)
I5	2.77 x 10^{-8} (8%)	3.04 x 10^{-7} (91%)	3.45 x 10^{-9} (1%)
L1	1.91 x 10^{-6} (6%)	8.20 x 10^{-5} (94%)	5.77 x 10^{-9} (0%)
L5	1.37 x 10^{-6} (8%)	1.48 x 10^{-5} (92%)	5.14 x 10^{-9} (0%)
GQ1	5.44 x 10^{-9} (13%)	1.24 x 10^{-9} (3%)	3.50 x 10^{-8} (84%)
GQ5	5.26 x 10^{-9} (17%)	1.44 x 10^{-9} (5%)	2.49 x 10^{-8} (78%)
GW1	3.24 x 10^{-5} (1%)	1.14 x 10^{-2} (99%)	4.46 x 10^{-5} (0%)
GW5	7.97 x 10^{-6} (2%)	4.14 x 10^{-4} (98%)	4.35 x 10^{-7} (0%)

to the UR, pointing out the potential dominance of PDI over the other two SEU mechanisms.

For the ISSI SRAM, the contributions to the UR (both in absolute and percentage terms) are reported in Table VII for both the MC simulations and for the approximated Dodds' method. PDI UR for GEO quiet conditions is found to contribute for a maximum of 11% to the total UR, again pointing out that PDI effects can be considered negligible in this environment. For the other three environments, when considering the MC simulations, PDI is still the major contributor to the UR. However, it is not dominant in all the cases. At the lowest, PDI contributes to 65% for the I5 orbit and can reach 97% for the GW1 environment. The situation is quite different when considering the approximated Dodds' method. In this case, PDI never contributes less than 91% for each orbit, with a peak of 99% for GW1.

TABLE VIII
UR OF THE **CYPRESS SRAM** FROM PROTON INDIRECT AND DIRECT IONIZATION AND HEAVY IONS (WITH PERCENTAGE CONTRIBUTIONS TO THE TOTAL UR IN BRACKETS) FOR EIGHT COMBINATIONS OF ORBITS AND SHIELDING CONFIGURATIONS. UR IN SEU/BIT/DAY.

Monte-Carlo			
Env.	**UR$_{HEP}$ (%)**	**UR$_{LEP}$ (%)**	**UR$_{HI}$ (%)**
I1	1.58 x 10^{-7} (8%)	1.88 x 10^{-6} (91%)	4.02 x 10^{-8} (1%)
I5	1.21 x 10^{-7} (21%)	4.17 x 10^{-7} (73%)	3.58 x 10^{-8} (6%)
L1	7.46 x 10^{-6} (5%)	1.37 x 10^{-4} (95%)	1.63 x 10^{-7} (0%)
L5	7.32 x 10^{-6} (23%)	2.41 x 10^{-5} (77%)	5.37 x 10^{-8} (0%)
GQ1	2.98 x 10^{-8} (11%)	1.14 x 10^{-9} (0%)	2.44 x 10^{-7} (89%)
GQ5	2.66 x 10^{-8} (12%)	2.31 x 10^{-10} (1%)	1.87 x 10^{-7} (87%)
GW1	2.70 x 10^{-4} (2%)	1.54 x 10^{-2} (96%)	3.34 x 10^{-4} (2%)
GW5	7.21 x 10^{-5} (11%)	5.48 x 10^{-4} (88%)	4.29 x 10^{-6} (1%)
Approximated Dodds' method			
Env.	**UR$_{HEP}$ (%)**	**UR$_{LEP}$ (%)**	**UR$_{HI}$ (%)**
I1	2.03 x 10^{-7} (6%)	3.41 x 10^{-6} (93%)	4.02 x 10^{-8} (1%)
I5	1.48 x 10^{-7} (14%)	8.65 x 10^{-7} (83%)	3.58 x 10^{-8} (3%)
L1	1.02 x 10^{-5} (4%)	2.33 x 10^{-4} (96%)	1.63 x 10^{-7} (0%)
L5	7.31 x 10^{-6} (15%)	4.20 x 10^{-5} (85%)	5.37 x 10^{-8} (0%)
GQ1	3.09 x 10^{-8} (11%)	3.54 x 10^{-9} (1%)	2.44 x 10^{-7} (88%)
GQ5	2.99 x 10^{-8} (14%)	4.10 x 10^{-9} (2%)	1.87 x 10^{-7} (84%)
GW1	1.73 x 10^{-4} (1%)	3.25 x 10^{-2} (98%)	3.34 x 10^{-4} (1%)
GW5	4.25 x 10^{-5} (4%)	1.18 x 10^{-3} (96%)	4.29 x 10^{-6} (0%)

For the Cypress SRAM, the contributions to the UR (both in absolute and percentage terms) are reported in Table VIII for both the MC simulations and for the approximated Dodds' method. In this case as well, PDI contributes to the GQ UR by 0-2%, pointing out that PDI will not contribute to the total UR in this environment. For the other three environments, when considering MC simulations, PDI is the main contributor to the UR and it is never below 73% and it can peak at 96% for the GW1 environment. One peculiarity for the Cypress SRAM is that the high-energy proton component of the UR is, in percentage, higher than for the other two memories. Similar to the ISSI SRAM, when considering the approximated Dodds' method the PDI contribution to the UR becomes dominant, with a 83% lowest percentage contribution for the I5 orbit and a maximum of 98% for the GW1 environment.

The D-factors for the RADSAGA 65 nm SRAM for both the MC and the approximated Dodds' methods are reported in Fig. 7. The plot is made to compare how the D-factor changes with orbit, shielding and calculation method. The RADSAGA 65 nm SRAM shows quite consistent D-factors for almost all the orbits when calculated either using MC or with the approximated Dodds' method. Letting the GEO quiet conditions aside, no matter the calculation method, the orbit or the shielding, the D-factor is never below 5 and can reach up to 43 for the L1 and GW5 orbits.

The D-factors for the ISSI SRAM for both the MC and the approximated Dodds' method are reported in Fig. 8. Note that, in this case, the data are reported in logarithmic scale to improve readability. In the case of the ISSI SRAM the two methods may disagree by even a factor of 4 for the I5 and GW1 environments. The approximated Dodds' method predicts the highest D-factor to be roughly 150 (for the GW1

This article has been accepted for publication in a future issue of this journal, but has not been fully edited. Content may change prior to final publication. Citation information: DOI 10.1109/TNS.2021.3061209, IEEE Transactions on Nuclear Science

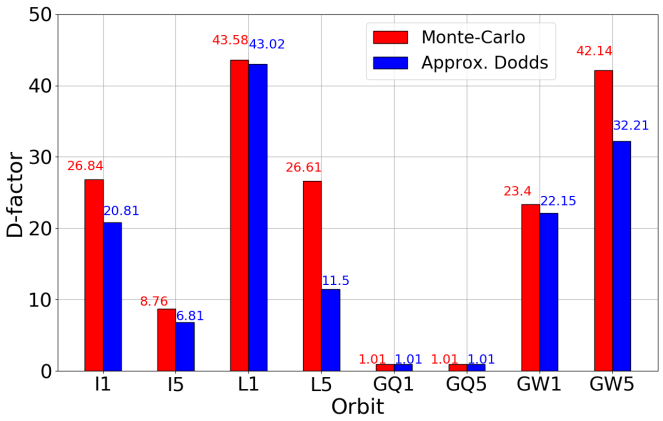

Fig. 7. D-factors of the RADSAGA 65 nm SRAM calculated for eight combinations of orbit and shielding with the MC simulations and the approximated Dodds' method.

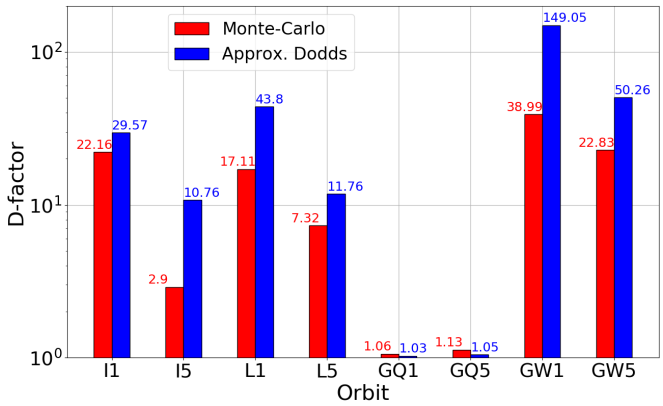

Fig. 8. D-factors of the ISSI SRAM calculated for eight combinations of orbit and shielding with the MC simulations and the approximated Dodds' method.

environment). For that same orbit, the MC simulations predicts a factor of 39. The minimum D-factors are found for the GQ conditions (just above 1). Letting this environment aside, the minimum would otherwise be 3 for the I5 orbit. For this same orbit, the approximated Dodds' method provides the lowest D-factor, which is as high as 11.

The D-factors for the Cypress SRAM for both the MC and the approximated Dodds' method are reported in Fig. 8, also in logarithmic scale. The comparison between the two methods yields similar observations as for the ISSI SRAM, though the difference, in this case, is moderate, i.e., the approximated Dodds' method yields less than a factor of 2 higher D-factors than MC for the ISS and LEO cases, with the only exception of GEO worst day. With the expection of the GQ cases, for which the D-factor is 1 or just above, all other D-factors are higher than 5. For MC, the highest D-factor is 27 for the GW1 orbit and the lowest is 4 for the I5 orbit. For the approximated Dodds' method, the highest D-factor is 65 for the GW1 orbit and the lowest is 6 for the I5 orbit.

The two methods point out quite heterogeneous contributions to the UR. In general, the MC simulations bring factors which are equal or lower than the approximated Dodds' method. Despite representing the most optimistic prediction

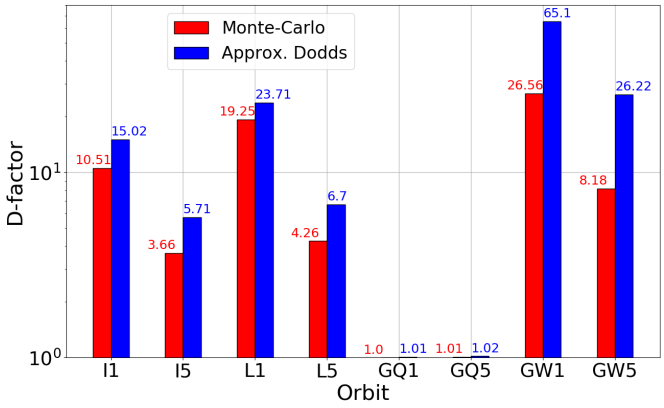

Fig. 9. D-factors of the Cypress SRAM calculated for eight combinations of orbit and shielding with the MC simulations and the approximated Dodds' method.

case, the MC simulations still yield D-factors that violate the safety margin of 5 established in the literature [10].

The shielding is almost always seen to provide a benefit in terms of UR in absolute value. However, it does have a quite limited impact on the D-factors. At best, for the ISSI SRAM, the D-factor for I5 was 7 times smaller than for I1. For the other conditions, the effect is no higher than a factor of 2. The RADSAGA 65 nm SRAM and the GEO stormy environment represent the only exception. For this only case, the D-factor for 500 mils is seen to be higher than for 100 mils for both methods. The reason is likely related to the wider PDI cross-section peak of the RADSAGA 65 nm SRAM with respect to the other two devices, which render the RADSAGA 65 nm SRAM also more sensitive to intermediate-energy protons. Hence, 500 mils of aluminum are likely not enough to mitigate the effects of a large part of the intermediate-energy protons. In the literature [38], more realistic shielding configurations were found to yield a reduction in the PDI UR by up to a factor of 25 with respect to the spherical 100 mils aluminum shielding.

VI. D-Factor as a Function of the Critical Charge

One advantage of the MC simulations is that they provide data over a wide range of critical charges. While losing the link to the data of these specific devices such analysis can allow exploring how the D-factor would vary when changing the critical charge of the model, which can be used to assess whether the device may be sensitive to direct ionization from high-energy protons and how the picture may change for other devices having a different critical charge. Note that the other parameters of the modelled SVs may also play a role, so this analysis will focus strictly on common observations among devices and models.

In order to use the MC data as a function of critical charge, the L1 orbit was chosen. The heavy ion contribution to the UR was found to be negligible for this orbit. This allows neglecting the overestimated (but still negligible) low-LET heavy ion response from MC, so that the D-factor simplifies further:

$$D(Q_{crit}) = \frac{UR_{HEP}(Q_{crit}) + UR_{LEP}(Q_{crit})}{UR_{HEP}(Q_{crit})} \qquad (2)$$

This article has been accepted for publication in a future issue of this journal, but has not been fully edited. Content may change prior to final publication. Citation information: DOI 10.1109/TNS.2021.3061209, IEEE Transactions on Nuclear Science

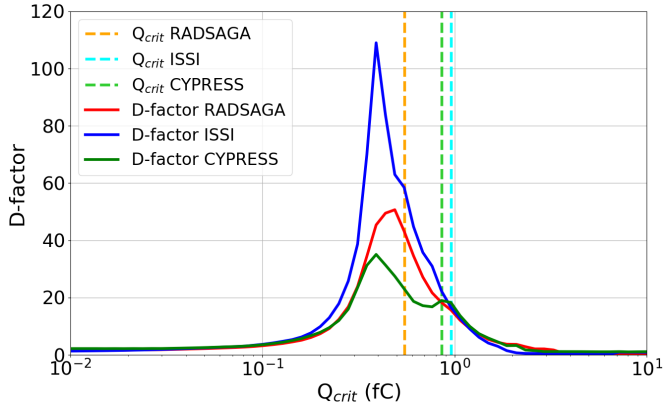

Fig. 10. D-factors of the three devices calculated for the LEO orbit with 100 mils of Aluminum shielding with the MC simulations as a function of the critical charge.

In general terms, the D-factor will converge to 1 at high critical charge because low-energy protons would not deposit enough charge to trigger SEUs. At the same time, it will converge to 1 also at very low critical charge (below 0.1 fC) because such a device would also be sensitive to direct ionization from high-energy protons. The latter would be covered through high-energy proton testing and would make the low-energy proton contribution less important in relative terms.

Thus, the D-factor is expected to reach an absolute maximum, usually at critical charges in between 0.1-1 fC. If the chosen critical charge is lower than that corresponding to the absolute maximum direct ionization effects may be relevant also at energies above 20 MeV.

Fig. 10 reports the D-factor as a function of critical charge for the three devices under consideration. For the RADSAGA 65 nm SRAM, the chosen critical charge falls very close to the peak region (which is at around 0.5 fC). This shows that this device is likely sensitive to direct ionization effects above 3 MeV and, potentially, up to 20 MeV.

For the ISSI SRAM, the chosen critical charge is just placed at the onset of the range of critical charges for which PDI becomes dominant. However, the ISSI SRAM shows an absolute maximum that can stretch up to more than 100.

The Cypress SRAM has the lowest peak in absolute value among the three devices. Another peculiarity is represented by the secondary peak located at the chosen critical charge (0.86 fC), for which the D-factor reaches a relative maximum, which is as high as 60% of the absolute maximum at 0.4 fC. The chosen critical charge (0.86 fC) places the model almost halfway between the absolute maximum and the onset, indicating that direct ionization from high-energy protons is unlikely for this device.

In general, the critical charge at which the D-factor reaches the absolute maximum is seen not to vary much among the different SV models and it occurs for a critical charge of 0.4-0.5 fC. However, the absolute value of the D-factor may vary by far, from 35 for the Cypress SRAM to 110 for the ISSI SRAM and it seems to be strictly related to the ratio between the PDI cross-section peak and the high-energy proton saturation cross-section observed experimentally.

VII. Discussion

The three devices under consideration have all proven, to different extents, to be very susceptible to direct ionization from low-energy protons. Experiments with mono-energetic protons exhibit ratios between the peak PDI cross-sections and the high-energy saturation cross-sections higher than 10^4.

When brought into an environmental context, such high and wide PDI effects were predicted to provide not only a significant contribution to the total UR, but, in most of the cases, they dominated the total UR response. No matter the prediction method used, the considered orbit or the shielding, PDI was found to contribute about 90% of the total UR on average, with maxima of 99%.

The corresponding D-factors calculated for these devices in the considered environments were always on the order of a few tens, reaching maximum values above 100 for the worst-case orbits. These were either Low-Earth orbits for which the trapped proton fluxes are quite high or the Geostationary orbit environments under the intensification of the proton fluxes provided by a strong solar activity. Shielding (varying from 100 to 500 mils of Al) was seen to have an impact, but just to a limited extent, often sufficient to reduce the D-factor by a factor of 2.

The D-factor is assumed to be a safety margin that one can apply to the UR calculated through Weibull fitting of the high-energy proton and heavy ion experimental cross-sections. It is clear that safety margins make sense if they are small compared to the quantity that is margined. At least for the considered devices, this is not the case for basically any space environment (even the supposedly mild ISS environment). Considering the potential uncertainty of the UR calculation methods for PDI effects, a method based on the application of safety margins over the UR calculated from high-energy protons and heavy ions is unlikely to work. Bounding the UR with the highest D-factor found among all the devices would mean applying always a factor of 150 to the UR calculated excluding low-energy protons, which will often be unrealistically pessimistic.

From the experimental data reported in other works [6, 13] it is clear that such a safety margin would provide a huge overshoot over the actual contribution of PDI to the UR of memory devices in general. More than providing a revision to the required safety margins to account for PDI when calculating the UR from high-energy proton and heavy ion responses, the presented data rather reinforce the need to perform experimental characterization of memory devices with either mono-energetic low-energy protons [31] or degraded high-energy proton beams [6].

Some further considerations can be made on the accuracy of the proposed calculation methods. The RPP models calibrated over low- and high-energy protons proved to be very accurate for the two proton contributors, but provided some overestimation of the heavy ion contribution with respect to the Weibull-predicted UR, which in turn would have reduced the D-factor. However, for the RADSAGA 65 nm SRAM the D-factor would have not reduced by more than a factor of 1.5, still pointing out a quite strong PDI enhancement.

Concerning the approximated Dodds' method, it is clear that it would not exactly correspond to the experimental measurements attained by degradation of a high-energy beam. However, this approximated method is likely not overestimating the UR by more than a factor of 5. Even when considering such a strong inaccuracy, it would still yield D-factors higher than 10 for certain devices and certain orbits.

In this respect, the simplicity of the approximated Dodds' method is counterbalanced by a higher degree of inaccuracy in the upset rate prediction, whereas the Monte-Carlo simulations can be considered to provide a higher-fidelity estimation within a factor of $\pm$ 2.

As a matter of fact, it will not be possible to draw conclusion about the accuracy of current UR prediction methods for PDI unless the devices are actually tested in the space environment. Currently, the devices analysed in this work have been considered for launch in LEO space missions. If proven to be that sensitive to the actual space radiation environment they could be considered as a baseline to have very sensitive radiation monitors to characterize the low-energy proton fluxes in space.

The analysis of the D-factor as a function of critical charge showed that for the RADSAGA 65 nm SRAM the worst-case scenario was already reached, being the chosen critical charge so close to that of the D-factor absolute maximum. This may point out an influence from direct ionization above 3 MeV, potentially extending up to 20 MeV and above. The analysis for the other two devices showed that they are still positioned at about the onset of the PDI sensitivity and still quite far from the absolute maximum.

VIII. Conclusions

Novel data and soft error prediction methods on the impact of PDI in SRAMs based on deep sub-micron technology and bulk Si were presented to report on the strong enhancement to the UR that would come from the observed PDI effects. The big impact seems to be related to both the relatively high peak PDI cross-section, compared to the high-energy proton saturation cross-section, and to the wide energy range for which direct ionization phenomena play a role, which may extend even above 3 MeV.

No matter the calculation method employed, PDI contributes, on average, about 90% of the total UR. The resulting safety margins (D-factors) to be applied to the UR calculated from high-energy protons and heavy ion experimental data generally exceed the factor of 5 previously established in the literature and can get as high as 150. Although, the analysed devices could just represent a worst case for PDI, it is suggested to pursue experimental characterization for PDI effects whenever the heavy ion LET threshold of the device is lower than 0.4 MeV/(mg/cm^2), rather than stick to the application of a general safety margin.

IX. Acknowledgments

We acknowledge Yolanda Morilla and Pedro Martìn-Holgado from CNA, Heikki Kettunen, Mikko Rossi and Jukka Jaatinen from RADEF, Marc-Jan van Goethem, Harry Kiewiet, Emil van der Graaff and Sytze Brandenburg from KVI-CART, Wojtek Hajdas, Laura Sinkunaite and Miroslaw Marszalek from PSI for their support during data collection at the respective facilities.

Special thanks to Helmut Puchner, from Cypress Semiconductors, for providing the information required to disable the embedded ECC within the Cypress 65 nm chip.

References

[1] K.P. Rodbell, D.F. Heidel, H.H.K. Tang, M.S. Gordon, P. Oldiges, and C.E. Murray, "Low-energy proton-induced single-event-upsets in 65 nm node, silicon-on-insulator, latched and memory cells," *IEEE Trans. Nucl. Sci.*, vol. 54, no. 6, pp. 2474-2479, December 2007.

[2] D.F. Heidel et al., "Low energy proton single-event-upset test results on 65 nm SOI SRAM," *IEEE Trans. Nucl. Sci.*, vol. 55, no. 6, pp. 3394-3400, December 2008.

[3] M.P. King et al., "Electron-induced single event upsets in static random access memories," *IEEE Trans. Nucl. Sci.*, vol. 60, no. 6, pp. 4122-4129, December 2013.

[4] B.D. Sierawski et al., "Muon-induced single event upsets in deppe-submicron technology," *IEEE Trans. Nucl. Sci.*, vol. 57, no. 6, pp. 3273-3278, December 2010.

[5] ESCC 25100, "Single event effects test method and guidelines," European Space Components Coordination, ESA.

[6] N.A. Dodds et al., "Hardness assurance for proton direct ionization-induced SEEs using a high-energy proton beam," *IEEE Trans. Nucl. Sci.*, vol. 61, no. 6, pp. 2904-2914, December 2014.

[7] A. Akkerman, J. Barak, and N.M. Yitzhak, "Role of elastic scattering of protons, muons, and electrons in inducing single event upsets," *IEEE Trans. Nucl. Sci.*, vol. 64, no. 10, pp. 2648-2660, August 2017.

[8] P. Caron, C. Inguimbert, L. Artola, R. Ecoffet, and F. Bezerra, "Physical mechanisms of proton-induced single-event upsets in integrated memory devices," *IEEE Trans. Nucl. Sci.*, vol. 66, no. 7, pp. 1404-1409, July 2019.

[9] Z. Wu, S. Chen, J. Yu, J. Chen, P. Huang, and R. Song, "Recoil-ion-induced single event uspets in nanometer CMOS SRAM under low-energy proton radiation," *IEEE Trans. Nucl. Sci.*, vol. 64, no. 1, pp. 654-664, January 2017.

[10] N.A. Dodds et al., "The contribution of low-energy protons to the total on-orbit SEU rate," *IEEE Trans. Nucl. Sci.*, vol. 62, no. 6, pp. 2440-2451, December 2015.

[11] B.D. Sierawski et al., "Impact of low-energy proton induced upsets on test methods and rate predictions," *IEEE Trans. Nucl. Sci.*, vol. 56, no. 6, pp. 3085-3092, December 2009.

[12] J.R. Schwank et al., "Hardness assurance testing for proton direct ionization effects," *IEEE Trans. Nucl. Sci.*, vol. 59, no. 4, pp. 1197-1202, August 2012.

[13] J. Guillermin, N. Sukhaseum, P. Pourrouquet, N. Chatry, F. Bezerra, and R. Ecoffet, "Worst-case proton contribution to the direct ionization SEU rate," *in Proc. 2017 RADECS Conf.*, Geneva, Switzerland, Sept. 2017, pp. 330-337.

[14] R. Garcia Alia et al., "Direct ionization impact on accelerator mixed-field soft error rate," *IEEE Trans. Nucl. Sci.*, vol. 67, no. 1, pp. 345-352, January 2020.

[15] J. Wang, J. Prinzie, A. Coronetti, and P. Leroux, "Study of the SEU sensitivity of an SRAM-Based Radiation Monitor in a 65-nm CMOS Technology," *submitted for publication in IEEE Trans. Nucl. Sci.*

[16] A. Coronetti et al., "SEU characterization of commercial and custom-designed SRAMs based on 90-nm technology and below," *in IEEE Radiation Effects Data Workshop Rec.*, Santa Fe, NM, USA, Dec. 2020, pp. 56-63.

[17] N.A. Dodds et al., "New insight gained on mechanisms of low-energy proton-induced SEUs by minimizing energy straggle," *IEEE Trans. Nucl. Sci.*, vo. 62, no. 6, pp. 2822-2829, December 2015.

[18] Y. Morilla et al., "Progress of CNA to become the spanish facility for combined irradiation testing in aerospace," *in Proc. 2018 RADECS Conf.*, Gothenburg, Sweden, Sept. 2018, pp. 250-254.

[19] A. Virtanen, R. Harboe-Sorensen, A. Javanainen, H. Kettunen, H. Koivisto, and I. Riihimaki, "Upgrades for the RADEF facility," *in IEEE Radiation Effects Data Workshop Rec.*, Honolulu, HI, USA, July 2007, pp. 38-41.

[20] H. Kettunen et al., "Low energy protons at RADEF - application to advanced eSRAMs," *in IEEE Radiation Effects Data Workshop Rec.*, Paris, France, July 2014, pp. 147-150.

[21] E.R. van der Graaf, R.W. Ostendorf, M.J. van Goethem, H.H. Kiewiet, M.A. Hofstee, and S. Brandenburg, "AGORFIRM, the AGOR facility for irradiations of material," *in Proc. 2009 RADECS Conf.*, Bruges, Belgium, Sept. 2009, pp. 451-454.

[22] W. Hajdas, F. Burri, C. Eggel, R. Harboe-Sorensen, and R. de Marino, "Radiation effects testing facilities in PSI during implementation of the PROSCAN project," *in IEEE Radiation Effects Data Workshop Rec.*, Phoenix, AZ, USA, July 2002, pp. 160-164.

[23] C. Weulersee, F. Miller, D. Alexandrescu, E. Schaefer, and R. Gaillard, "Assessment and comparison of the low-energy proton sensitivity in 65nm to 28nm SRAM devices," *in Proc. 2011 RADECS Conf.*, Seville, Spain, Sept. 2011, pp. 291-296.

[24] N. Seifert, B. Gill, J.A. Pellish, P.W. Marshall, and K.A. LaBel, "The susceptibility of 45 and 32 nm bulk CMOS latches to low-energy protons," *IEEE Trans. Nucl. Sci.*, vol. 58, no. 6, pp. 2711-2718, December 2011.

[25] R.K. Lawrence, J.F. Ross, N.F. Haddad, R.A. Reed, and D.R. Albrecht, "Soft error sensitivities in 90 nm bulk CMOS SRAMs," *in IEEE Radiation Effects Data Workshop Rec.*, Quebec City, QC, Canada, July 2009, pp. 123-126.

[26] PSTAR, National Institute of Standards and Technology, https://physics.nist.gov/PhysRefData/Star/Text/PSTAR.html, accessed May 2020.

[27] J.F. Ziegler, and J.P. Biersack, "Stopping and range of ions in matter," http://www.srim.org, accessed August 2018.

[28] G. Battistoni et al., "Overview of the FLUKA code," *Annals of Nuclear Energy*, vol. 82, pp. 10-18, August 2015.

[29] T.T. Bohlen et al., "The FLUKA Code: Developments and Challenges for High Energy and Medical Applications," *Nuclear Data Sheets*, vol. 120, pp. 211-214, June 2014.

[30] B. Ye et al., "Low energy proton induced single event upset in 65 nm DDR and QDR commercial SRAMs," *Nucl. Instr. and Methods in Phys. Res. B*, vol. 406, pp. 443-448, September 2017.

[31] J.A. Pellish et al., "Criticality of low-energy protons in single-event effects testing of highly-scaled technologies," *IEEE Trans. Nucl. Sci.*, vol. 61, no. 6, pp. 2896-2903, December 2014.

[32] J.M. Trippe et al., "Predicting muon-induced SEU rates for a 28-nm SRAM using protons and heavy ions to calibrate the sensitive volume model," *IEEE Trans. Nucl. Sci.*, vol. 65, no. 2, pp. 712-718, February 2018.

[33] R.A Reed et al., "Impact of ion energy and species on single event effects analysis," *IEEE Trans. Nucl. Sci.*, vol. 54, no. 6, pp. 2312-2321, December 2007.

[34] CREME, Vanderbilt University, https://creme.isde.vanderbilt.edu, accessed May 2020.

[35] E.L. Petersen, J.C. Pickel, J.H. Adams, and E.C. Smith, "Rate prediciton for single event effects," *IEEE Trans. Nucl. Sci.*, vol. 39, no. 6, pp. 1577-1599, December 1992.

[36] E.H. Cannon et al., "Heavy-ion, high-energy and low-energy proton SEE sensitivity of 90-nm RHBD SRAMs," *IEEE Trans. Nucl. Sci.*, vol. 57, no. 6, pp. 3493-3499, December 2010.

[37] L.D. Edmonds, and K.J. Edmonds, "A method for estimating SEU rates from protons by direct ionization," *IEEE Trans. Nucl. Sci.*, vol. 55, no. 5, pp. 2666-2678, October 2008.

[38] J.A. Pellish et al., "Impact of spacecraft shielding on direct ionization soft error rates for sub-130 nm technologies," *IEEE Trans. Nucl. Sci.*, vol. 57, no. 6, pp. 3183-3189, December 2010.